OFFICE OF NAVAL RESEARCH

Contract N7onr-330-III

NR-064-121

Technical Report No. 3

A STUDY IN PHOTOPLASTICITY: THE PHOTOELASTIC EFFECT IN THE REGION OF LARGE DEFORMATION IN POLYETHYLENE

by

B. Fried and N. H. Shoup

DIVISION OF INDUSTRIAL RESEARCH
WASHINGTON STATE INSTITUTE OF TECHNOLOGY
STATE COLLEGE OF WASHINGTON
PULLMAN, WASHINGTON
May, 1953

A STUDY IN PHOTOPLASTICITY: THE PHOTOELASTIC EFFECT IN THE REGION OF LARGE DEFORMATION IN POLYETHYLENE

B. Fried and N. H. Shoup

INTRODUCTION

The work reported here is a continuation of investigations[1*] of the suitability of various materials for potential use in the extension of the photoelastic method of strain analysis to the region of large plastic deformations.

Earlier studies of the strain-optical effect in this range[2,3,4] have, in large part, been undertaken from the point of view of determining the physicochemical properties of macro-molecules rather than from the standpoint of its possible use as a tool in technical mechanics.

In Figures 1a, b, and c, the possible mechanical and optical properties of photoelastic materials are illustrated on a three-dimensional scale. The three coordinate axes are those of stress (σ), strain (ε), and optical retardation (r). Thus a space curve, $f(\sigma,\varepsilon,r)$, describing the mechanical and optical behavior of a material will have as its orthogonal projection on the σ-ε plane the stress-strain curve, $\Phi(\sigma,\varepsilon)$, of that material; on the σ-r plane the stress-retardation curve, etc. Figure 1a illustrates the case for which the projection of the curve $f(\sigma,\varepsilon,r)$ on the σ-r plane is a straight line representing a linear relationship between optical retardation and stress such as we have reported for cellulose nitrate under certain conditions of loading.[1] There are, however, many cases in which the deformations in the plastic range are of more significance than is the stress distribution which produces the deformation. For information of this kind, a material having the properties shown in Figure 1b, in which the optical retardation is a linear function of the strain, would have obvious advantages. Materials for which stress, strain, and retardation all vary with one another in a nonlinear manner (Figure 1c) have, in the absence of other considerations, little to recommend them for the proposed application.

In addition, suitable materials must have high optical sensitivity and stress-strain relationships not unlike those of real engineering materials. Polyethylene, satisfying these latter conditions, was therefore selected for further study.

SPECIMEN PREPARATION

Optical transparency and photoelastic uniformity of the polyethylene sheets available was of some concern since most samples exhibited a marked "frosted" pattern. These effects have been attributed to the growth of nuclei of crystallization, which frequently occurs during the slow cooling of the newly formed sheet, although this may presumably also result from ageing even at room temperatures.[5,6,7]

*Bibliography at end of paper.

Considerable improvement in both uniformity and clarity was attained by heating samples confined between strips of chrome-plated brass to the softening range (100°to 170°C) and then quenching the sample and platens in water at room temperature. A thin film of high-temperature silicone grease on the platens permitted easy separation of the polyethylene from the metal surfaces.

The problem was also brought to the attention of the American Agile Corporation, and they are now able to supply material generally suitable for testing purposes in the form of 6" x 6" sheets.

Specimens used in the calibration tests were formed by stamping with a cutter having hollow-ground knife edges (Figure 2).

CALIBRATION TESTS

The known dependence on strain rate $\dot{\varepsilon}$, of the mechanical properties of visco-elastic materials suggested the advisability of controlling the strain rate during the calibration tests. Further, in order to minimize the effects of both optical and mechanical creep, the strain rate would necessarily have to be rapid. These considerations required that the instrumentation be such that the stress, strain, and birefringence could be simultaneously and continuously recorded. Therefore, the instrumentation described below provides for autographic recording of these variables.

Continuous load measurements were made through use of a calibrated steel load beam as the sensitive element. Strain gauges of the SR-4 electrical resistance type were cemented to both the tension and compression sides of the beam and served to indicate the load in terms of a change in electrical resistance in two arms of an initially balanced A.C. bridge circuit. The resulting bridge unbalance is then amplified, and the amplified signal operates one channel of the recording oscilliograph.

The optical retardation is similarly recorded through the second channel of the oscillograph. Since the uniform test section of the calibration specimen is under a uniform tensile load, the optical effect is also uniform over this region. Thus the specimen will appear alternately light and dark in the polarized light field with increasing load or deformation. This cyclic variation in light intensity is picked up by a photocell, amplified, and the output signal is fed into the second channel of the recording oscilliograph. Each minima in the light intensity record corresponds to a fringe order, i.e., one wave length retardation in the specimen in a dark field polariscope, and each maxima corresponds to one-half wave length retardation.

Strain records were made with a "grating" strain gauge (Figure 3). The gratings were made by photographing a machine-ruled metal grating. The reduction in size available in the process was used to produce grating negatives with lines spaced 0.010 inch apart. Using two superimposed gratings, attached at appropriate gage lines on the specimen, the longitudinal extension of the specimen under load causes one grating to move relative to the other. A photocell is then employed to pick up the variations in light transmitted through the grating combination from a light source. With each ten thousandths relative movement of the gratings the photocell picks up one cycle of the alternate light-dark sequence. This cyclic signal is then amplified and recorded simultaneously with the load and optical retardation measurements. As only two-

channel oscillographs were available, the strain signal is recorded on a second two-channel oscillograph, and this chart is evenly marked with the load and optical retardation chart on the first oscillograph through time signals.

This arrangement (see Figure 4) provides the three above variables recorded as a function of time. A typical record is illustrated in Figure 5. The chart data are then plotted or computed to secure the separate relations between stress, strain, and optical retardation.

Typical tensile stress-strain curves for polyethylene at four different strain rates--from 0.022 in/in/min to 0.26 in/in/min in tension--are shown in Figure 6.

The strain rate, however, does not appear to influence the linear dependence of optical retardation on strain (see Figure 7).

Additional calibration tests were made under conditions of biaxial loading. Strains were measured from distortion of a grid printed directly on the test specimens. Results of these tests established the dependence of the optical retardation on the principal strain difference ($\varepsilon_1 - \varepsilon_2 = \gamma$) just as in the normal photoelastic case.

It should be remarked that the retardations plotted in Figure 7 are values which have been corrected for changes in specimen thickness. The magnitudes of the changes in thickness in the tensile specimen are indicated in Figure 8, where tensile strain is plotted versus the ratio of lateral to axial strain. Necessary corrections of observed retardations for changes in model thickness during deformation may become quite large.*

CREEP TESTS

Creep tests were run at 70°F and at a number of different stress levels during which simultaneous measurements were made of both optical retardation and strain as a function of time of loading. Results of these tests are shown in Figures 9 and 10.

The functional dependence of optical retardation on stress and time was found to be of the same form as that of the strain on the same variables. This result could have been anticipated from our calibration tests.

It is interesting to note that although in principle an equation of state cannot be expected to exist for real materials, it appears, in the present case, and within certain limits, that a reasonably good approximation to an equation of state may be assumed.

It is possible, for example, to construct a family of stress-strain curves with strain rate as the parameter from the creep curves of Figure 11. (The curves A', B', C', and D' correspond to the strain rates used in obtaining the stress-strain curves of Figure 7.) Points on this family of curves so obtained are indicated as plotted points in Figure 12 for comparison with the constant strain rate curves reproduced from Figure 7.

*Such corrections do not appear to have been made by some of the earlier investigators, nor does the dependence of optical retardation on shear strain rather than linear strain in polyethylene appear to have been recognized.

SIMILITUDE CONDITIONS IN THE PLASTIC RANGE

In order to apply the photo-plasticity method of analysis to problems of strain distribution in structural members made of engineering materials, one must have, in addition to geometric similitude, similarity of the stress-strain curves of the model and prototype materials.

Whether or not such similarity exists between the stress-strain curves of model and prototype materials can best be determined from nondimensional representations of these curves. Such nondimensional stress-strain curves have been drawn for the model material, polyethylene, and a prototype material, 3S aluminum sheet. The normal shear stress-shear strain curves for these materials are illustrated in Figures 13 and 14.

On the stress-strain curve* for the aluminum a secant modulus (G_A') was drawn to a point corresponding to the largest shear strain expected in the series of tests described in the following section. This point was at

τ_1 = 10,950 psi and γ_1 = 0.0145 and $G_A' / G_A' = \alpha = 0.189$.

The stress-strain curve was then replotted with τ/τ_1 as the ordinate scale and γ/γ_1 as abscissa.

A secant modulus was then drawn on the normal stress-strain curve for polyethylene with $G_P' = \alpha G_P$ which intersected the curve at τ_1 = 450 psi and γ_1 = 0.430. The dimensionless curve for polyethylene was then drawn to the same scale of τ/τ_1, and γ/γ_1, as the aluminum. As would be expected, and as is apparent from Figure 15, the two curves are not coincident at all points and are therefore not perfectly similar.

The tests described in the following section were designed to determine, nonetheless, how reliable the predicted behavior of the 3S material would be from photoplasticity data on polyethylene.

EXPERIMENTAL RESULTS FOR 3S ALUMINUM AND POLYETHYLENE

The selection of a problem for comparison of photoplasticity data with independent data taken directly from measurements on an aluminum prototype was made primarily on the basis of expediency and simplicity of instrumentation. The model structure was a long strip loaded in tension and containing a centrally located hole.

We limited ourselves to the determination of the shear strain distribution across the extension of the diameter of the hole transverse to the load. Along this axis the principal strains are parallel and normal to the direction of tension. Resistance strain gauges, SR-4 Type A-7, were mounted on the aluminum test member in the directions of these principal strains at five stations between the edge of the hole and the edge of the plate. Identical gauges were mounted on the shank of the strip at a section approximately seven diameters above the hole, again parallel and perpendicular to the direction of tension.

*In what follows the terms stress and strain, unless otherwise specifically noted, refer to shear stress and shear strain, respectively.

Principal strains at all staions were recorded for a number of values of principal strain in the uniformly strained shank.

Shear strain distributions across the same section in a geometrically similar polyethylene member were determined for several values of the shear strain in the shank using the usual methods of photoelasticity.

Comparisons between the shear strain distributions in the model and prototype should be made on the basis of equivalent shear strains in the uniform section. Since, however, the two nondimensional curves do not coincide in this region the "equivalent" strain in the polyethylene for a given strain in the aluminum is undefined. Calculations were therefore made for two postulated criteria of equivalence.

The first assumes equivalence when the ratio of the shear strains in the shanks (γ_s) to their respective critical shear strains (γ_1) are equal, i.e., $(\gamma_s/\gamma_1)_{\text{aluminum}} = (\gamma_s/\gamma_1)_{\text{polythylene}}$.

The second assumes equivalence when $(\tau_s/\tau_1)_{\text{aluminum}} = (\tau_s/\tau_1)_{\text{polyethylene}}$

Thus, we compare the shank conditions at point A on the aluminum curve in Figure 15 with those in the polyethylene at points B and C, respectively.

The results showing the strain distribution as measured in the aluminum and the predicted strain distribution from photoplasticity data for each of the above postulated criteria of equivalence are shown in Figure 16. It is important to note that the polyethylene curves have not been corrected for changes in optical path length, i.e., changes in model thickness under load, except at the edge of the hole.

DISCUSSION OF RESULTS

The results, as indicated in Figure 16, show good agreement between the strain gauge data taken from the aluminum prototype and the photoplasticity data taken from the polyethylene model using either of the two postulated criteria of equivalence between model and prototype.

It is not possible, within the limits of accuracy of our measurements, to determine "true" criteria of equivalence in the present case. However, at the edge of the hole where corrections were made for the changes in optical path length in the polyethylene, the average of the strain predicted from the two sets of optical data is in all cases within 5 per cent of the value obtained with aluminum. This agreement, in spite of the divergence of the stress-strain curves of the two materials, makes the photoplasticity technique appear very promising as an experimental method for studies of the inelastic behavior of stressed members.

The anticipated difficulties, arising from the fact that our model was strained at different rates across the section considered, did not appear. This may have resulted from the fact that the stress-strain curves for the polyethylene over the range of strain rates here experienced diverged less from one another than from the aluminum stress-strain curve.

At the present case, creep in the aluminum was not perceptible until loads were reached for which the "equivalent" polyethylene fringe patterns showed so many closely packed ringes that they could not be resolved.

From the point of view of simplicity of experimental technique, the photoplasticity method seems best adapted to solution of problems in plane strain rather than plane stress. For the latter application, it is necessary to make supplementary measurements of model thickness changes in order to correct for optical path lengths at all points in the model.

With the difficulties now encountered in obtaining clear, homogenous model material of sufficient thickness to resist buckling, even under comparatively low compressive stresses, there is a serious limitation placed on the scope of application of the proposed method. The potentialities of photoplasticity may not be fully evaluated or realized until such model material becomes available.

ACKNOWLEDGMENT

We wish to thank Dr. W. O. Baker of the Bell Telephone Laboratories for supplying us with samples of polyethylene prepared in his laboratory and for his helpful discussions concerning the properties of this material.

BIBLIOGRAPHY

1. B. Fried, "Some Observations on Photoelastic Materials Stressed Beyond the Elastic Limit," Proc. Soc. Exp. Stress Analysis, v 8, n , 1950, pp.143-148.

2. T. Alfrey Jr., Mechanical Behavior of High Polymers, New York, Interscience Publishers, 1948.

3. H. Kolsky and A. C. Shearman, "Photo-Elastic Investigations of Structural Changes in Plastic Materials," Proc. Physical Soc. (Lond.), v 55, part 5, Sept. 1943, pp. 383-395.

4. R. H. Carey, E. F. Schulz, and G. J. Dienes, "Mechanical Properties of Polyethylene," Ind. Eng. Chem., v 42, n 5, May 1950, pp. 842-847.

5. C. S. Fuller, W. O. Baker, and N. R. Pape, "Crystalline Behavior of Linear Polyamides," Journ. Amer. Chem. Soc., v 62, Dec. 1940, pp. 3275-3281.

6. W. O. Baker and C. S. Fuller, "Macromolecular Disorder in Linear Polyamides," Journ. Amer. Chem. Soc., v 64, 1942, pp. 2399-2407.

7. W. O. Baker and C. S. Fuller, "Thermal Evidence of Crystallinity in Linear Polymers," Ind. Eng. Chem., v 38, Mar. 1946, pp. 272-277.

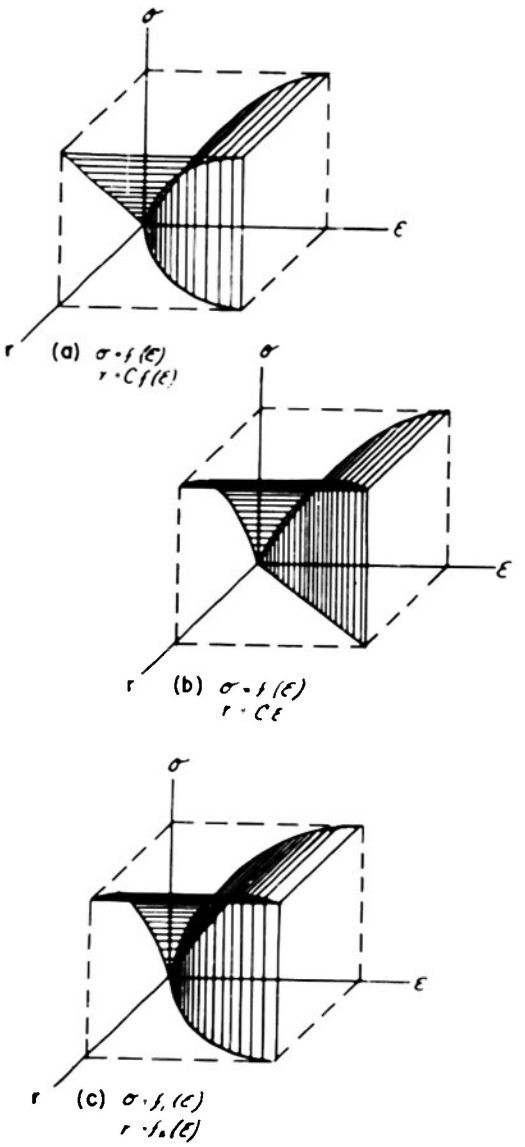

Fig 1 Possible stress-strain-optical behavior of photoelastic materials.

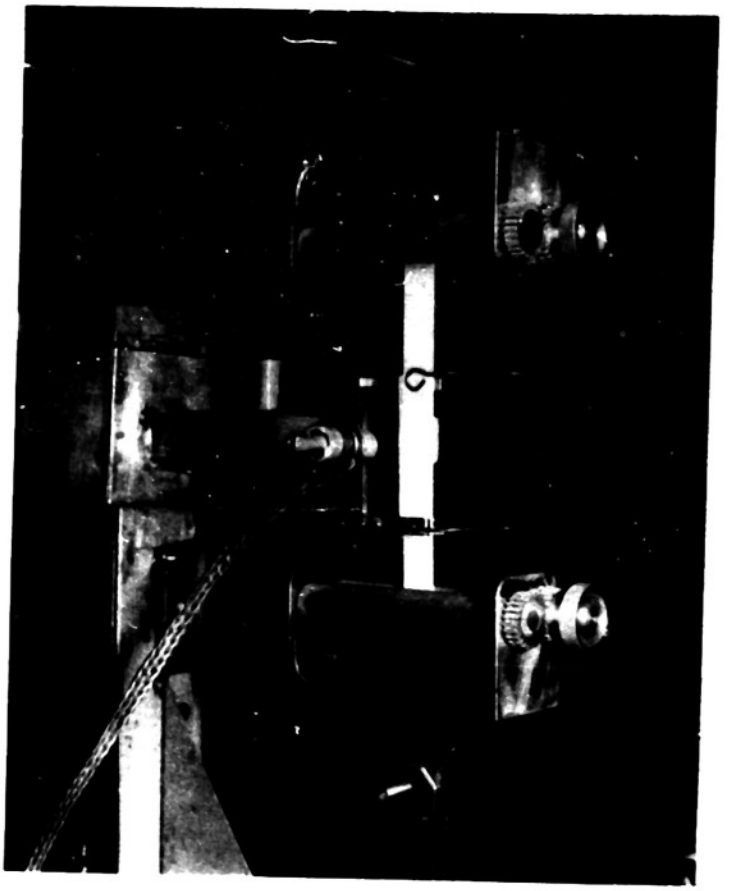

Fig. 3 Grating strain gage and photocell assembly

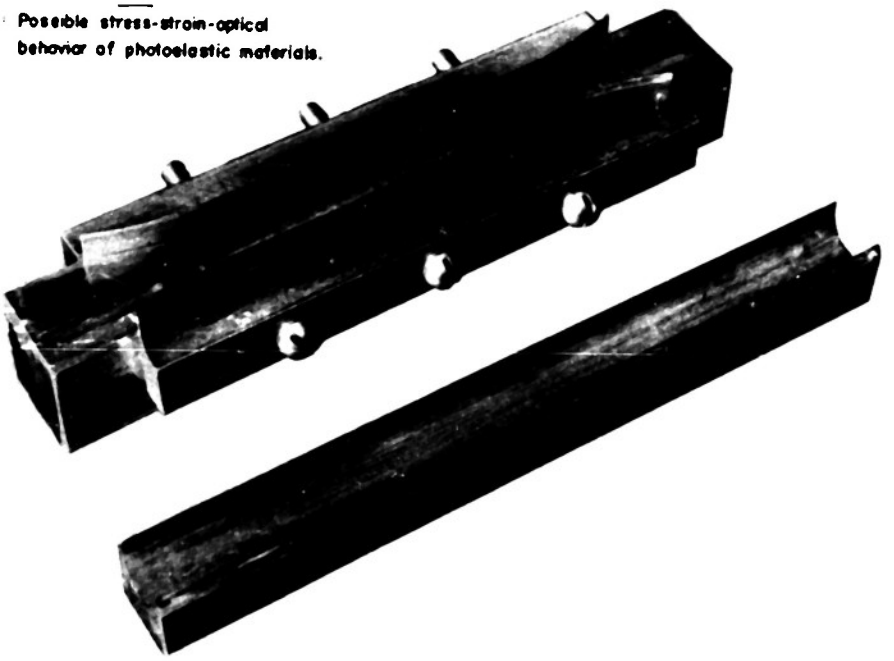

Fig. 2 Cutters for polyethylene specimens

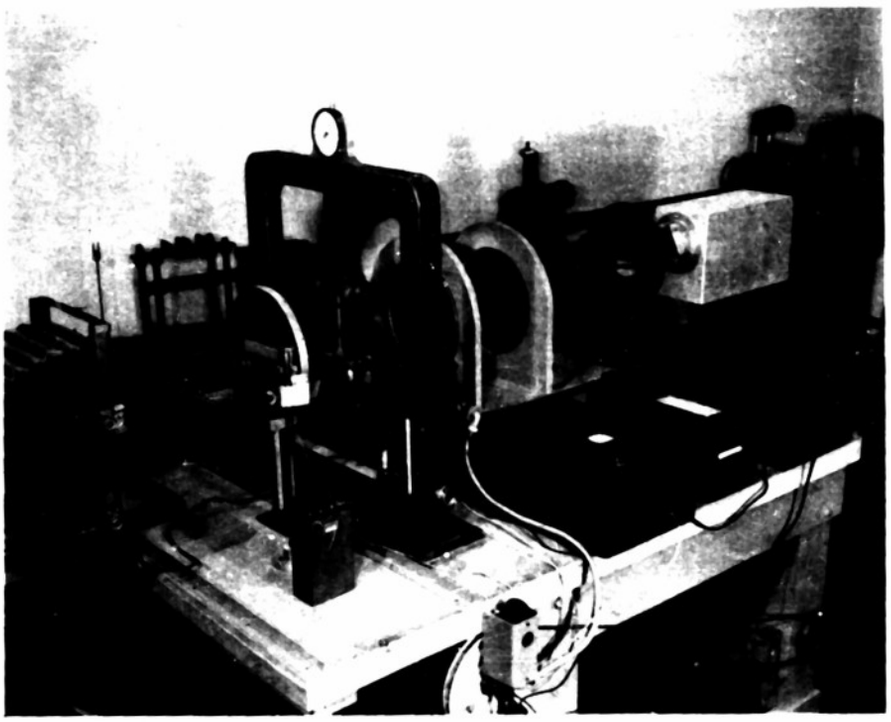

Fig. 4 Calibration test setup

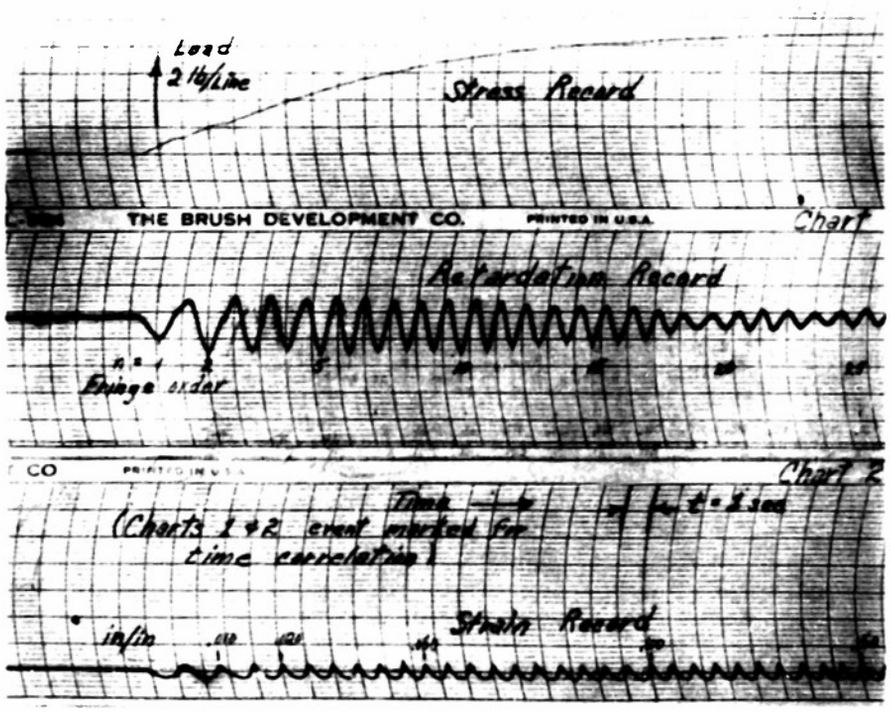

Fig. 5 Typical calibration test records

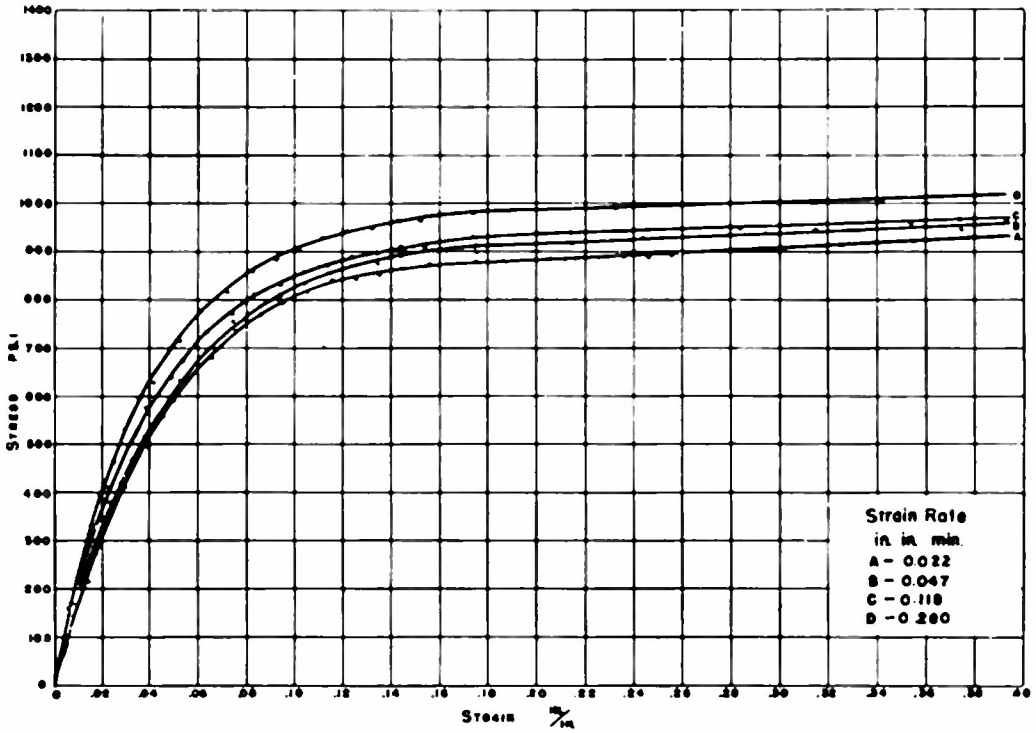

Fig. 6 Tensile stress-strain curves for polyethylene at a number of strain rates.

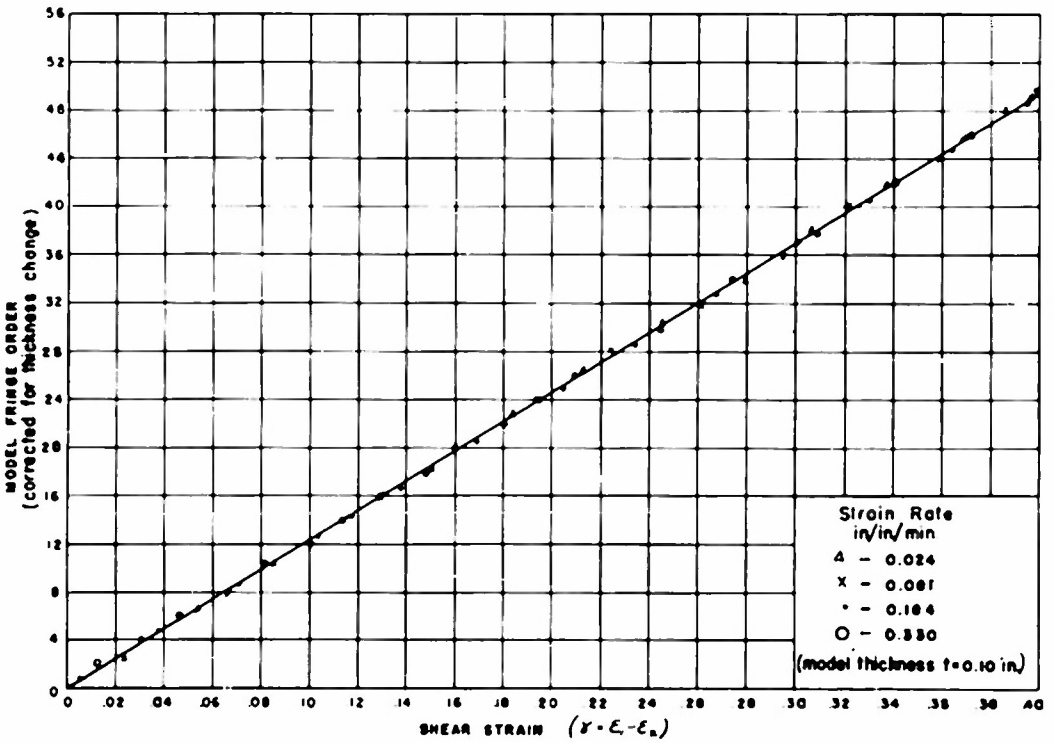

Fig.7 Optical retardation vs. shear strain for polyethylene

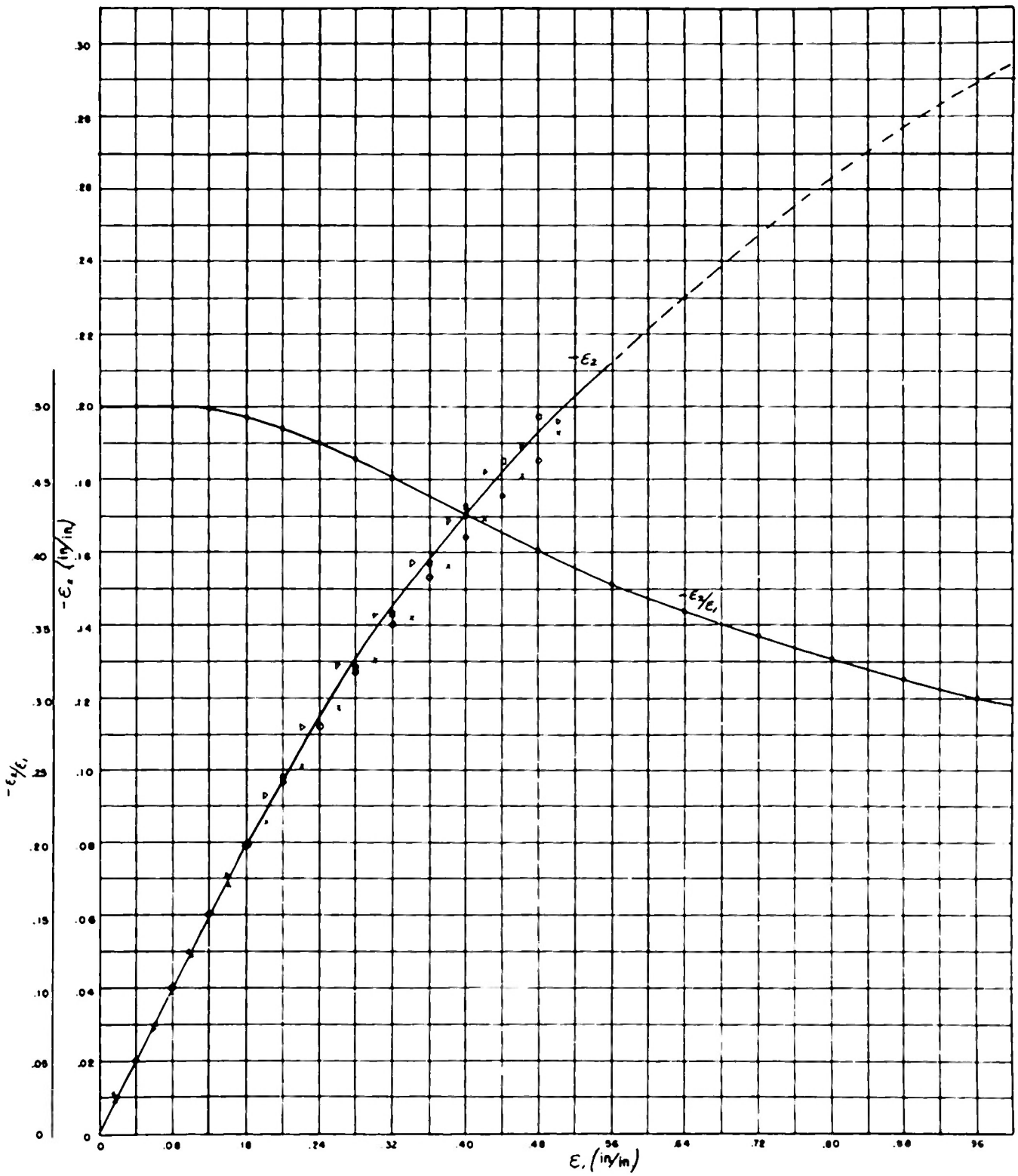

Fig. 8 Relations between principal strains in tensile calibration tests.

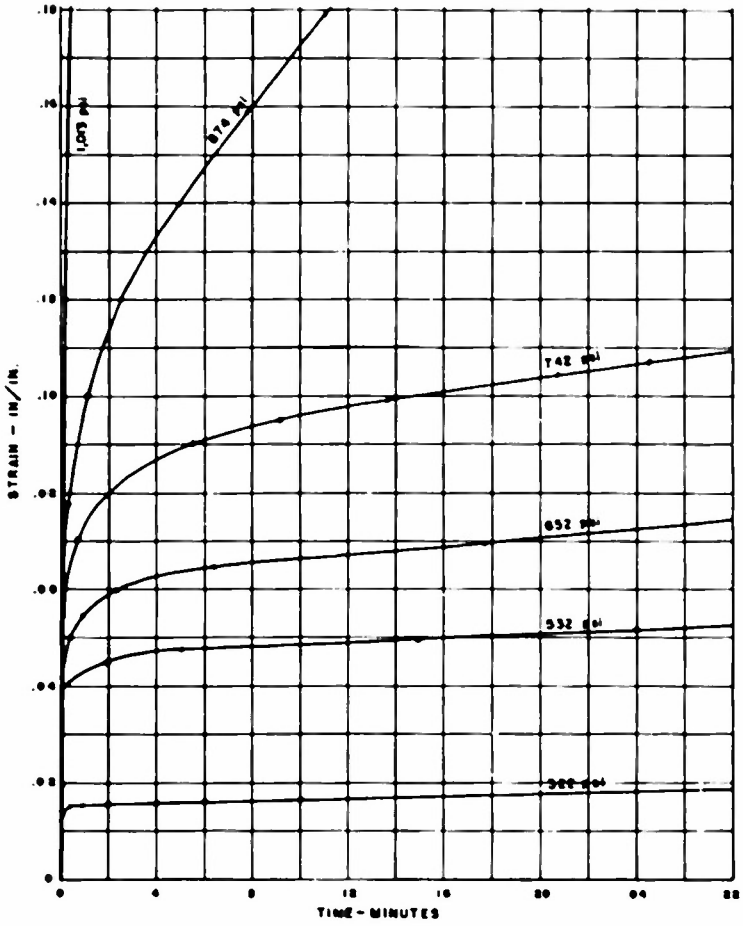

Fig. 9 Mechanical creep in polyethylene.

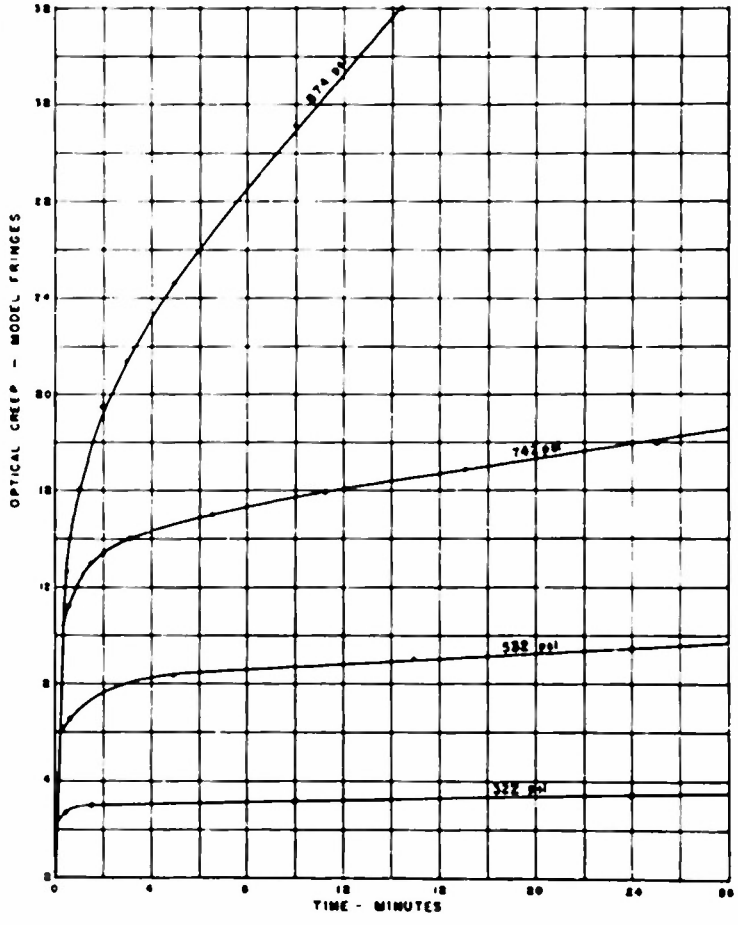

Fig. 10 Optical creep in polyethylene.

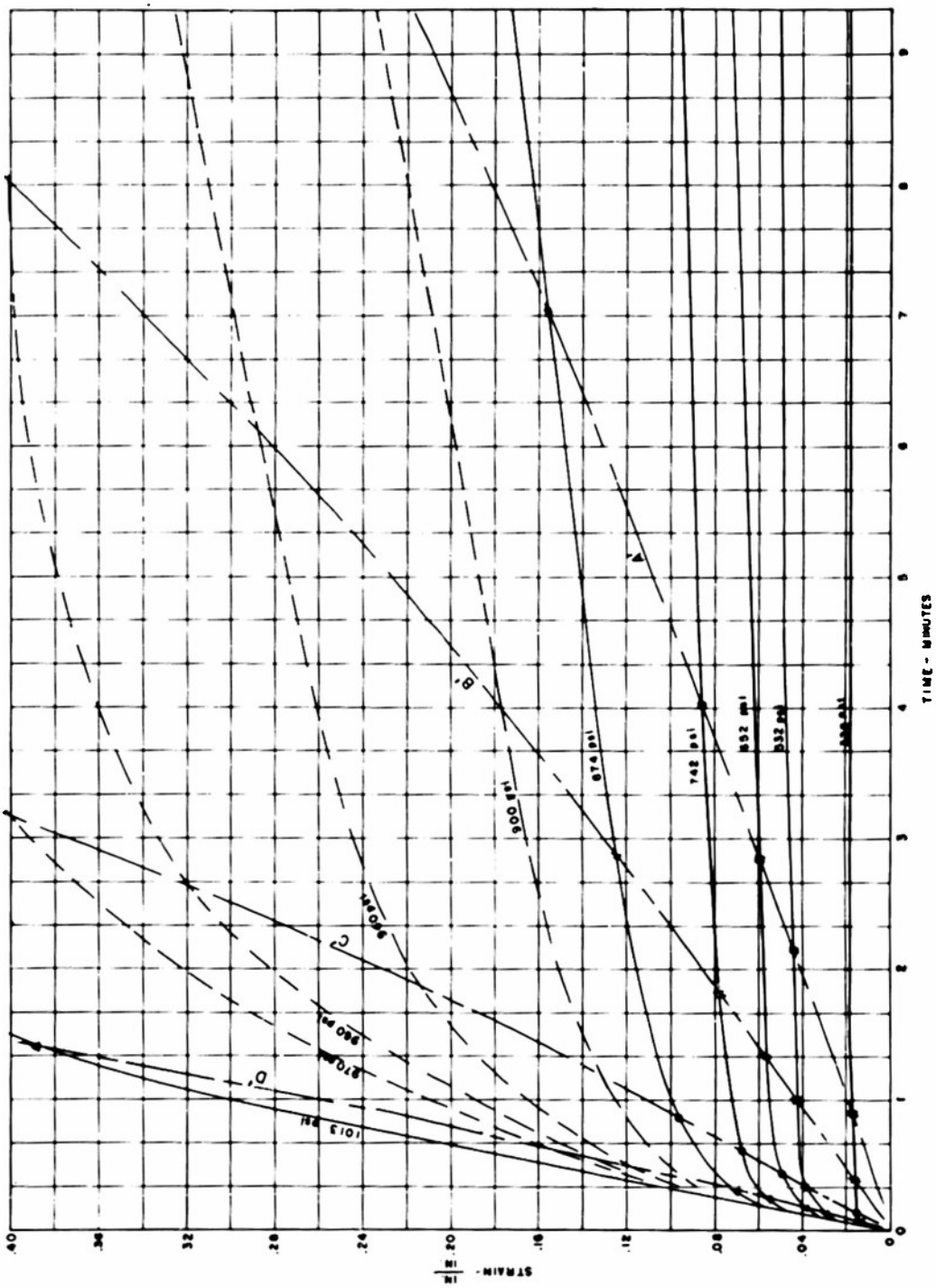

Fig. 11 Creep and calibration strain rate curves.

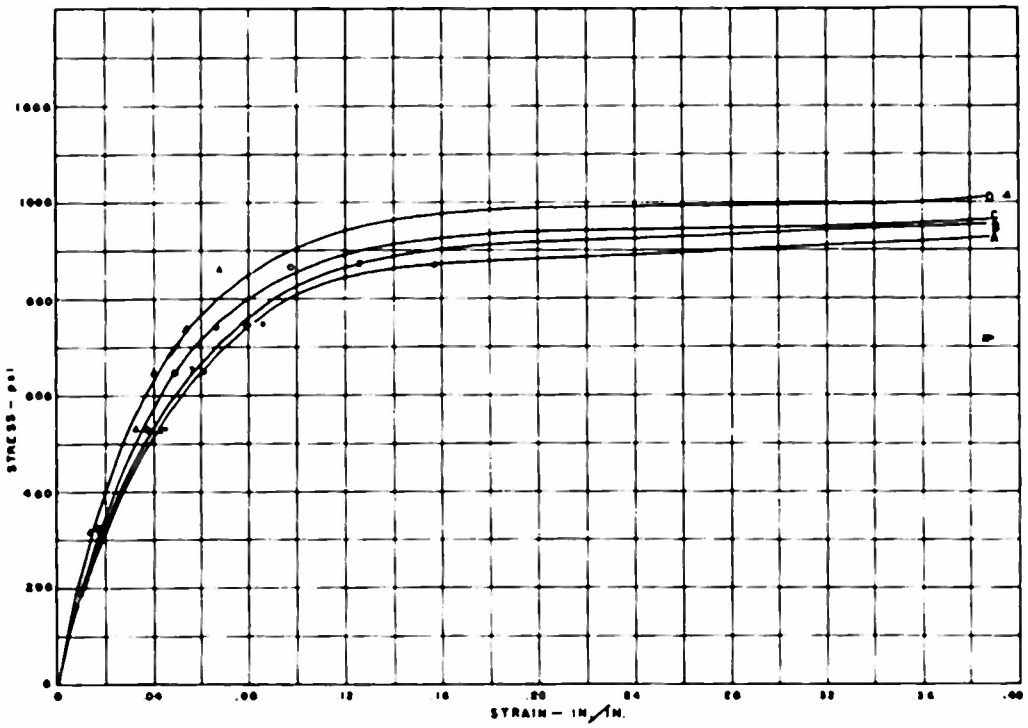

Fig. 12 Tensile stress-strain curves of fig. 7. Plotted points represent independent data for corresponding strain rates taken from creep data.

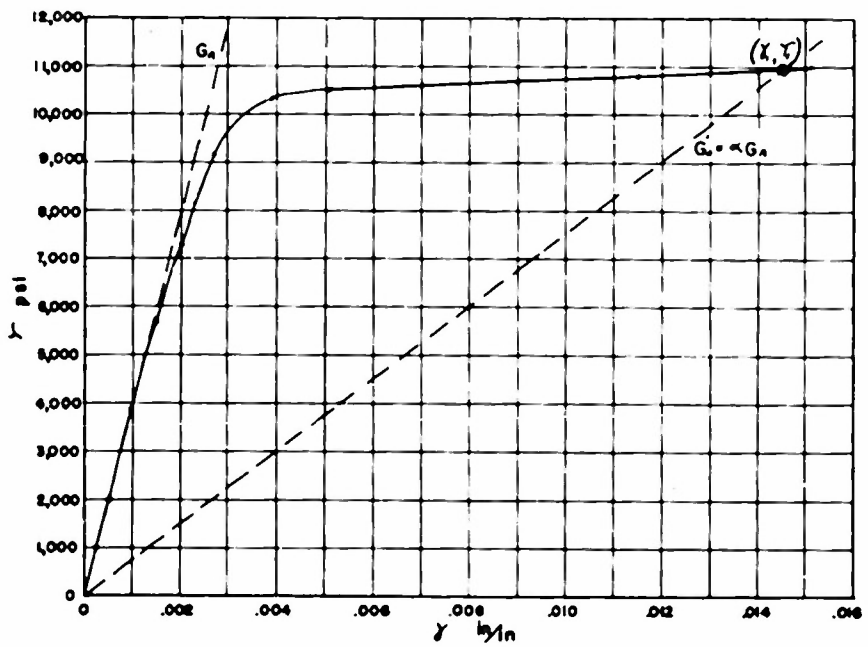

Fig. 13 Shear stress-strain curve for Aluminum.

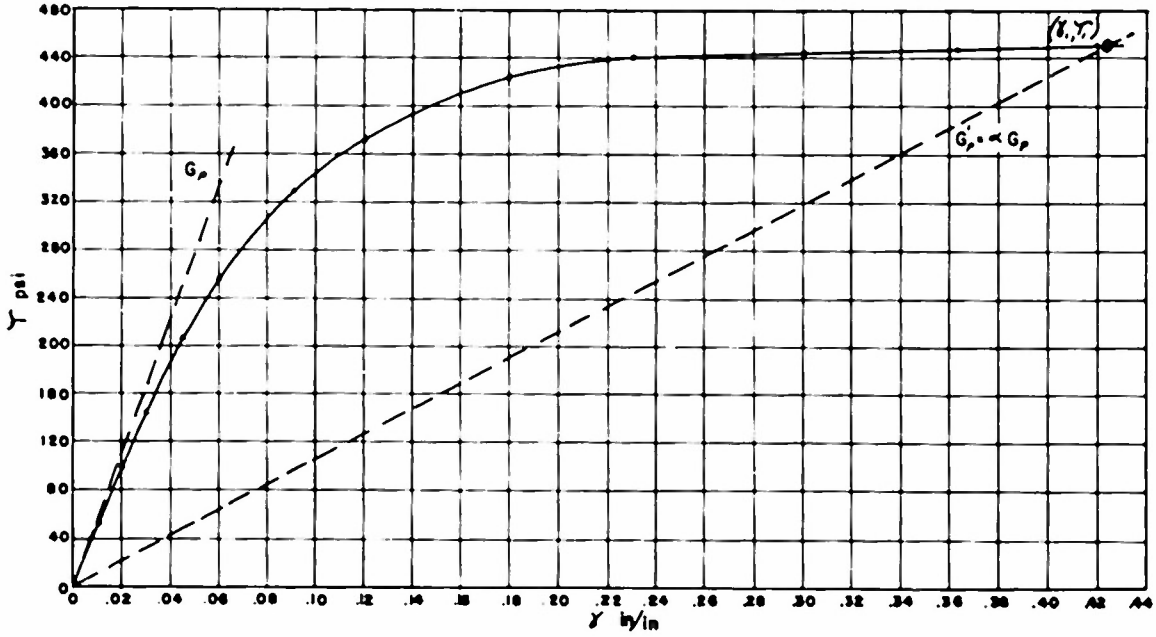

Fig. 14 Shear stress-strain curve for polyethylene.

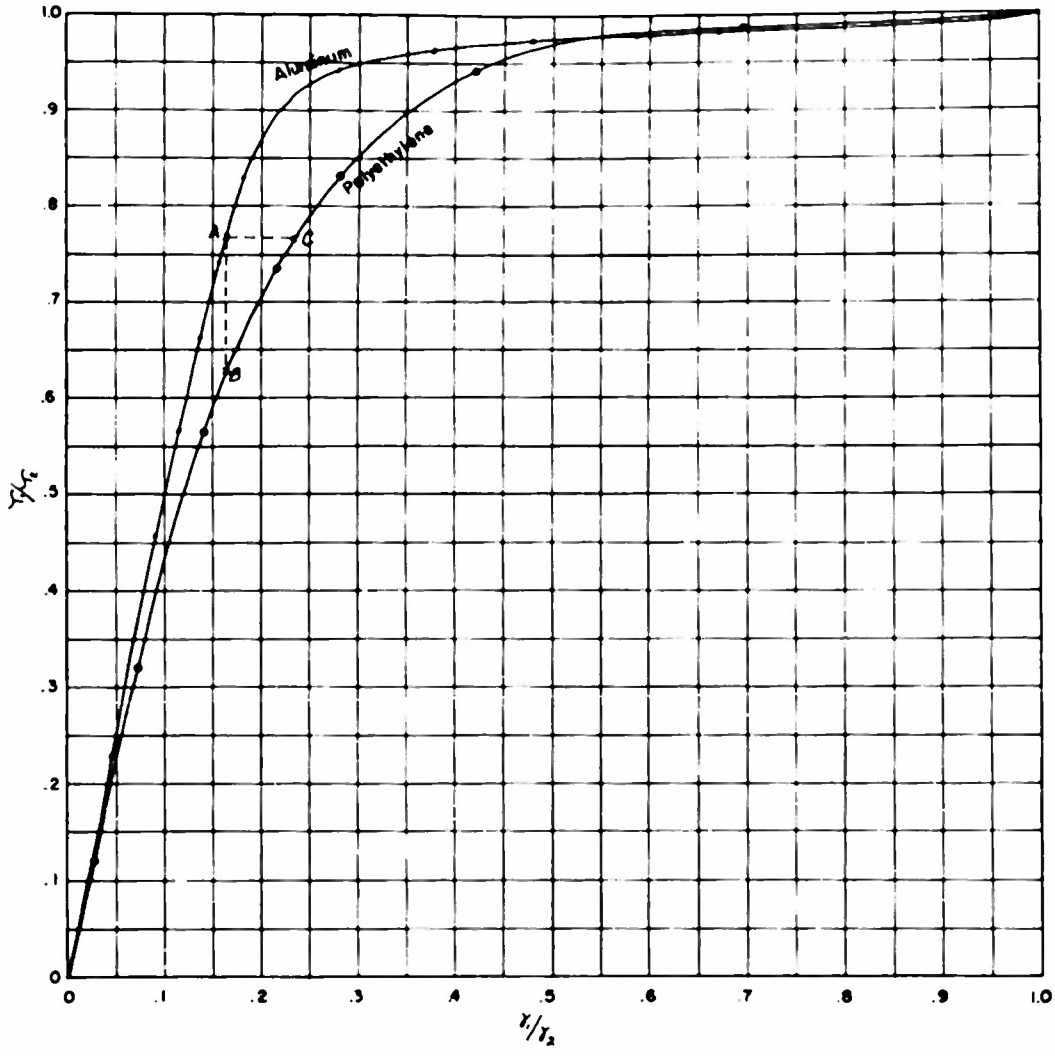

Fig. 15 Nondimensional plot of shear stress-strain curves for aluminum and polyethylene.

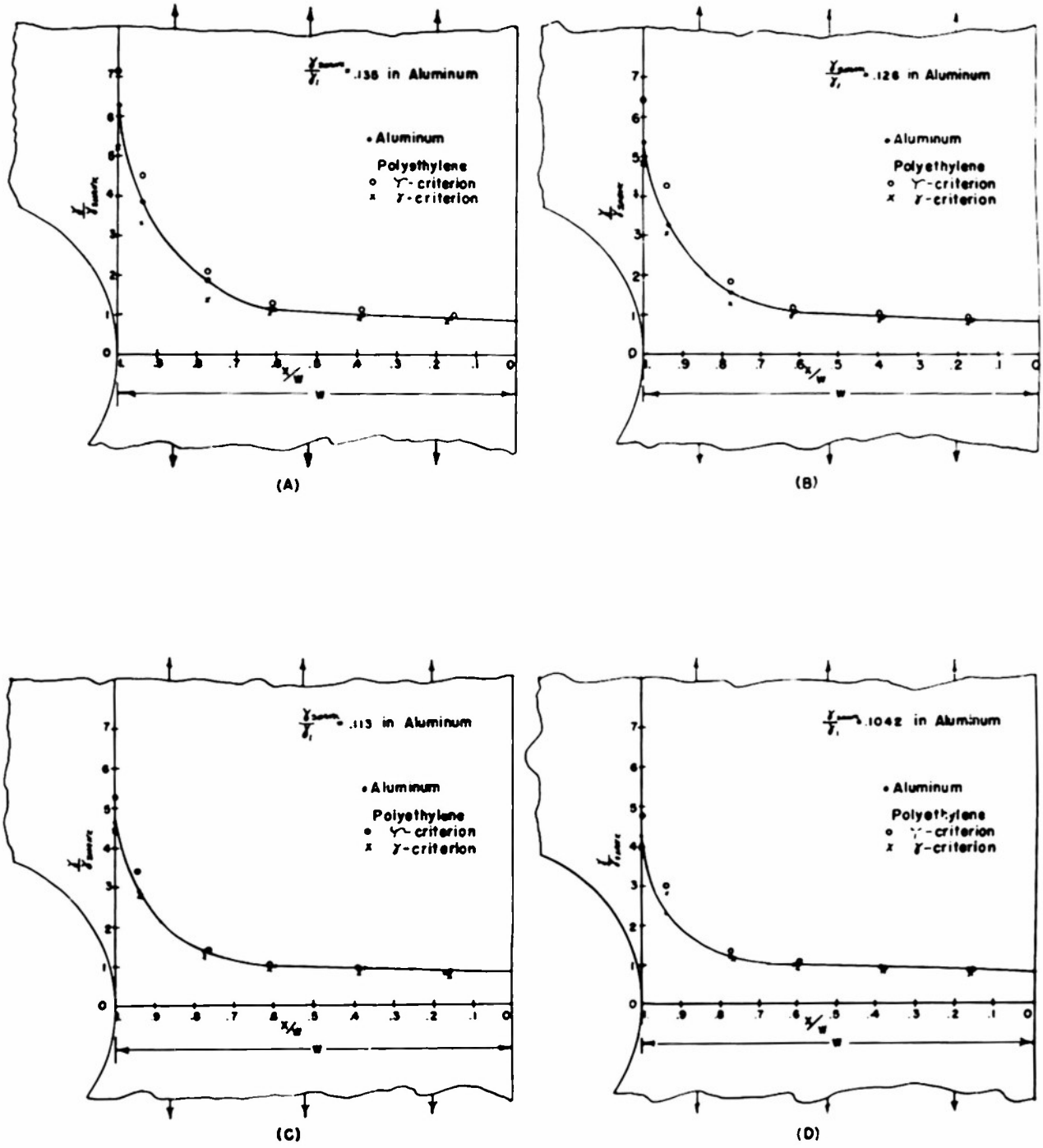

Fig. 16 Shear strain distribution across minimum section of axially loaded plate with central hole. Ratio of plate width to hole diameter, D/d, equals 4.

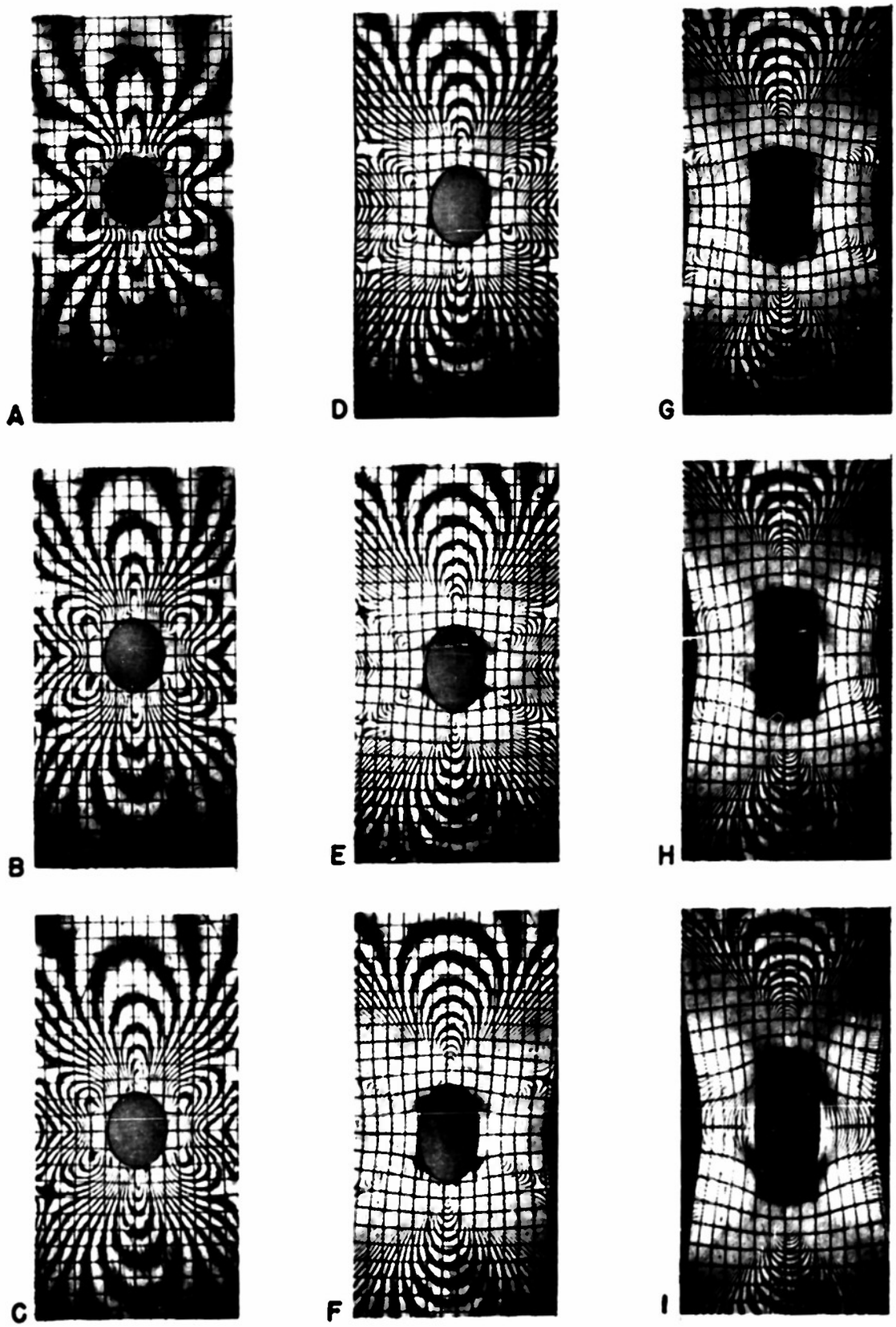

Fig. 17 Sequence of fringe patterns with increasing strain. Strains of larger magnitude than those in frame (D) are beyond the range considered in this paper. (D/d = 3)